J Appl Electrochem (2013) 43:1225–1233
DOI 10.1007/s10800-013-0610-x

RESEARCH ARTICLE

Preparation and capacitance performance of polyaniline/titanium nitride nanotube hybrid

Chi Xia · Yibing Xie · Yong Wang · Wei Wang · Hongxiu Du · Fang Tian

Received: 11 May 2013 / Accepted: 8 August 2013 / Published online: 18 August 2013

Abstract A polyaniline/titanium nitride (PANI/TiN) nanotube hybrid was prepared and used for an electrochemical supercapacitor application. Firstly, the well-aligned TiN nanotube array was prepared by anodization of titanium foil and subsequent nitridation through ammonia annealing. Then, PANI was deposited into TiN nanotube through the electrochemical polymerization process. The obtained PANI/TiN nanotube hybrid had an ordered porous structure. A high specific capacitance of 1,066 F g^{-1} was obtained at the charge–discharge current density of 1 A g^{-1} when only the mass of PANI was considered. The specific capacitance can even achieve 864 F g^{-1} at 10 A g^{-1} and still keep 93 % of the initial capacity after 200 cycles. An aqueous supercapacitor, consisting of two symmetric PANI/TiN nanotube hybrid electrodes and 1.0 M H_2SO_4 electrolyte solution, showed the specific capacitance of 194.8 F g^{-1}, energy density of 9.74 Wh kg^{-1}, and power density of 0.3 kW kg^{-1}.

Keywords Titanium nitride · Polyaniline · Nanotube hybrid · Electrochemical capacitance

1 Introduction

Electrochemical capacitors, also called supercapacitors, store energy by using either ion adsorption or fast surface redox reactions. They can complement batteries in electrical energy storage and harvesting applications when high power delivery or uptake is needed [1, 2]. A notable improvement in performance has been achieved through the development of advanced nanostructured electrodes. One-dimensional nanostructured materials (e.g., nanotube and nanowire array) have attracted much attention for electrochemical energy storage [3–9]. These nanostructured electrode materials contribute a high surface area for charge storage. Additionally, they serve as reliable electrical contacts for charge collectors [4]. Recently, self-organized titania nanotubes have been used as supercapacitor electrode materials, due to their semiconducting properties, accessible surface, electrochemical behavior, and long-term chemical stability [6, 7, 10, 11]. Such nanotube electrodes with large surface areas, high packing densities, and ordered pore networks facilitate rapid charge–discharge kinetics as well as a high power density [3–5]. Moreover, the nanotubes are in direct contact with the current collector and hence it is not necessary to use conducting additives and binders, which reduce both the weight and volume of the electrodes [3]. However, because of the poor electrical conductivity and poor electrochemical activity of TiO_2, anodic TiO_2 nanotube array shows a low specific capacitance [5]. It has been reported that both hydrogenated TiO_2 nanotube array and carbon-modified TiO_2 electrodes improve the electrical conductivity and stability of TiO_2 materials [4, 5, 10]. Moreover, titanium nitride is reported to possess oxidative stability, corrosion resistance, and good electrical conductivity, which make TiN an excellent candidate for electrochemical capacitors in highly corrosive electrolytes [6, 12, 13]. On the other hand, polyaniline (PANI) is considered to be one of the most promising electrode materials in pseudo-supercapacitors owing to its low cost, ease of synthesis, relatively high

C. Xia · Y. Xie (✉) · Y. Wang · W. Wang · H. Du · F. Tian
School of Chemistry and Chemical Engineering, Southeast University, Nanjing 211189, China
e-mail: ybxie@seu.edu.cn

C. Xia · Y. Xie · W. Wang · H. Du
Suzhou Research Institute of Southeast University, Suzhou 215123, China

theoretical capacitance, and flexibility [14–16]. Nevertheless, supercapacitors based on PANI are generally considered to be of poor cycling stabilities and high self-discharge rates [17]. Some available methods have been attempted by combining PANI with various types of carbon materials [18, 19]. The hybrid of PANI with carbon nanotubes has been proposed as an effective approach to improve the mechanical and electrochemical properties of electrodes [19, 20]. The preparation of ordered carbon nanotubes requires accurate and complicated control technology [21].

In this study, a simple approach is proposed to prepare a PANI/TiN nanotube hybrid by electrodepositing PANI into highly ordered TiN nanotubes. The TiN nanotubes are used as current collectors to decrease the internal resistance of the PANI and provide high intrinsic surface area. The PANI covered on TiN nanotubes can avoid the cycling degradation caused by volume changes and can also contribute to high pseudo-capacitance performance. The PANI/TiN nanotube hybrid with high specific capacitance, superior rate capability, and good stability becomes a promising electrode material for electrochemical capacitive energy storage application.

2 Experimental

2.1 Preparation of TiN nanotube array

TiO_2 nanotube array was synthesized by electrochemical anodization of a Ti sheet (purity of 99.7 %, thickness of 0.5 mm). Prior to anodization, the Ti sheet was cleaned by ultrasonication in acetone, ethanol, and then deionized water successively. Then, Ti sheet was anodized at 60 V for 3 h, using an ethylene glycol electrolyte solution containing 0.074 M NH_4F and 0.55 M water [22]. The as-prepared TiO_2 nanotube array was thoroughly washed with ethanol and deionized water, and dried in air. The sample was annealed in air at 450 °C for 1 h. Finally, the TiN nanotube array was obtained by annealing TiO_2 nanotube array in a tubular furnace at 800 °C for 2 h under ammonia atmosphere with a flow rate of 40 mL min^{-1} [6].

2.2 Preparation of PANI/TiN nanotube hybrid

The PANI/TiN nanotube hybrid was electrochemically synthesized using a standard three-electrode setup, which includes a TiN nanotube/Ti foil (1.5 cm × 4.0 cm) as the working electrode, a Pt plate as the counter electrode, and a saturated calomel electrode (SCE) as the reference electrode. Aniline was distilled under vacuum condition for purification treatment. The aqueous electrolyte solution contained 0.1 M aniline monomer and 1 M sulfuric acid. Prior to the electrochemical experiments, the electrolyte was deoxygenated by bubbling with N_2 for 10 min. Electrochemical polymerization of aniline was carried out using the normal pulse voltammetry method [23]. The pulse potential was increased from 0.55 to 0.85 V with a pulse potential increment of 0.001 V. The pulse width was 3 S and the pulse period was 9 S. After electro-polymerization reaction, the PANI/TiN nanotube hybrid was washed with distilled water and ethanol and was dried under air flow. The mass of deposited polymer was calculated by measuring the weight difference of TiN nanotube before and after the deposition of PANI using an electronic balance to an accuracy of 0.1 mg. Herein, the loading amount of PANI on PANI/TiN nanotube hybrid was 2.0 mg, which was equal to 0.33 mg cm^{-2}.

2.3 Structure characterization

The surface morphology and microstructure of the bare TiO_2 nanotube, TiN nanotube, and PANI/TiN nanotube hybrid were investigated using scanning electron microscopy (SEM, Hitachi S-3000, Japan). Raman spectroscopy was performed on a Raman spectrometer (Raman, Oceanoptics Benchtop Raman System, USA) using a He–Ne laser emitting at 785-nm excitation in the wave number range of 0–2,000 cm^{-1}. X-ray diffraction (XRD patterns) was recorded with a Bruker-AXS Microdiffractometer (D8 ADVANCE, Germany) using Cu-Ka radiation source.

2.4 Electrochemical measurement

The electrochemical performance of the PANI/TiN electrode material was investigated by cyclic voltammetry and electrochemical impedance spectrum in a three-electrode configuration. A Pt plate was used as the counter electrode and a saturated calomel electrode (SCE) was used as the reference electrode. The cyclic voltammetry was measured in a potential range of 0–0.6 V (vs. SCE) using a CHI760C electrochemical workstation (CHI760C, CH Instruments, USA). Electrochemical impedance (EIS) spectrum was recorded in a frequency range of 0.05–100,000 Hz with the ac potential amplitude of ±5 mV using the electrochemical workstation (IM6e ZAHNER Elektrik, Germany). The open potential was controlled at 0 V and 0.5 V (vs. SCE). The electrochemical capacitance was investigated through the galvanostatic charge–discharge measurement using the battery testing system (PAR VersaSTAT3 Electrochemical Analyzer). All electrolytes used above were 1 M H_2SO_4 aqueous solution. The specific capacitance (C), energy (E), and power (P) densities are calculated using the following equations [24]:

$$C = \frac{Q}{\Delta V \times m} = \frac{I \times t}{\Delta V \times m} \quad (1)$$

$$E = \frac{I \times t \times \Delta V}{2m} = \frac{C \times (\Delta V)^2}{2} \quad (2)$$

$$P = \frac{I \times \Delta V}{2m} \quad (3)$$

where C is the specific capacitance, I is the charge–discharge current, t is the time of discharge, ΔV is the voltage difference between the upper and lower potential limits, and m is the mass of active materials. Alternatively, m is the sum mass of both electrodes in a supercapacitor application.

3 Results and discussion

3.1 Preparation and morphology characterization

The applied pulse potential curve in the pulse voltammetry deposition process is shown in Fig. 1a. Generally, the electro-polymerization reaction is a kinetics-controlled process. The oxidation of aniline, which initially occurred at approximately 0.71 V, results in nucleation of PANI. The subsequent polymerization reaction of aniline can take place at a lower potential due to the self-catalytic effect of PANI [15, 16]. In this study, the pulse potential increment was controlled from 0.55 to 0.85 V. A short pulse width of 3 s and a long pulse period of 9 s were applied for this electrochemical synthesis, which could benefit the molecular diffusion of aniline monomers into the TiN nanotube template.

Figure 1b shows the current response curve when synthesizing PANI/TiN nanotube hybrid. The corresponding current density is only below 1 mA cm^{-2} when the initial potential increases from 0.55 to 0.71 V, which indicates inactive behavior of the work electrode. A quick enhancement of current density can be then achieved when the electrode potential is further raised from 0.73 to 0.85 V, which indicates PANI formation on the TiN nanotube substrate. At the terminate potential of 0.85 V, the current density is about 16 mA cm^{-2}. When the electro-polymerization reaction is conducted at a higher terminal potential, the electrolyte would be turned into light green due to the high growth rate of PANI. It restrains the further growth of PANI on the TiN nanotube substrate and leads to inferior capacitance performance of PANI.

Figure 2a and b shows that TiO_2 nanotubes are vertically aligned on a Ti foil. The average nanotube pore diameter and the wall thickness are about 80 and 20 nm, respectively. The nanotube length is about 4 μm. Figure 2c and d shows that the TiN nanotubes and TiO_2 nanotubes

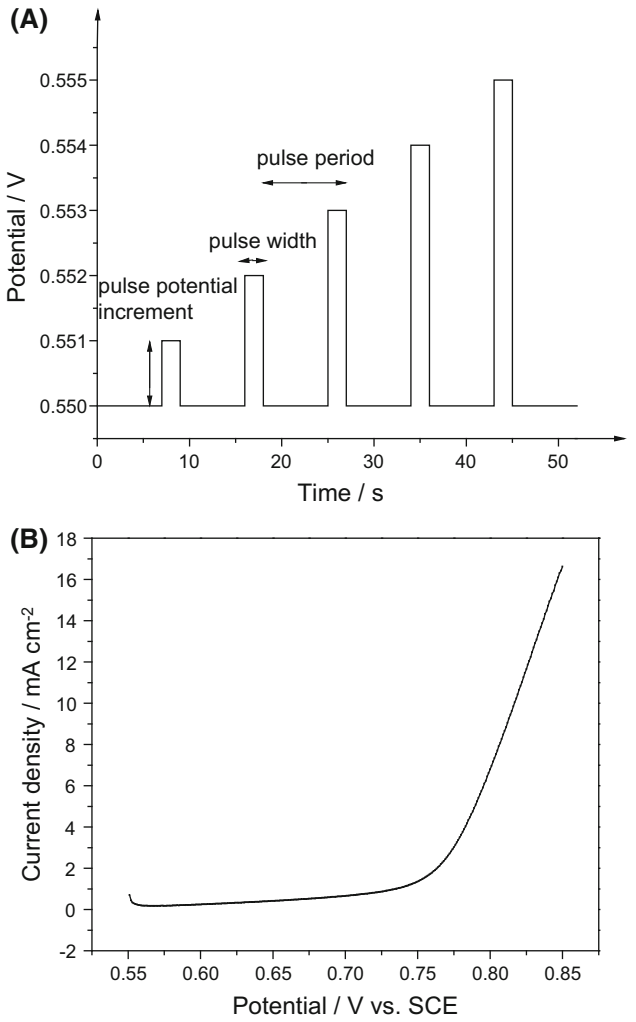

Fig. 1 **a** The applied pulse potential curve and **b** the responding current curve in a normal pulse voltammetry deposition process to synthesize PANI/TiN nanotube hybrid

have similar pore sizes and tube lengths. It means that there are no obvious morphological changes after TiO_2 conducts thermal treatment at 800 °C for 2 h in ammonia atmosphere [13]. Figure 2e and f shows that PANI fills the entire TiN nanotube and intertube space. The densely packed PANI film is covered on the tube mouth. The coaxial heterojunction of TiN nanotube and PANI is well constructed to form a top-porous network structure. This ordered porous structure can make full utilization of the electroactive PANI and the nanostructured current collector of TiN nanotube, which is beneficial for supercapacitor application. Actually, pyrrole monomers diffuse into the TiN nanotube and intertube space. The polymerization occurs along the nanotube walls until polymer coats the top surface of the nanotube [25].

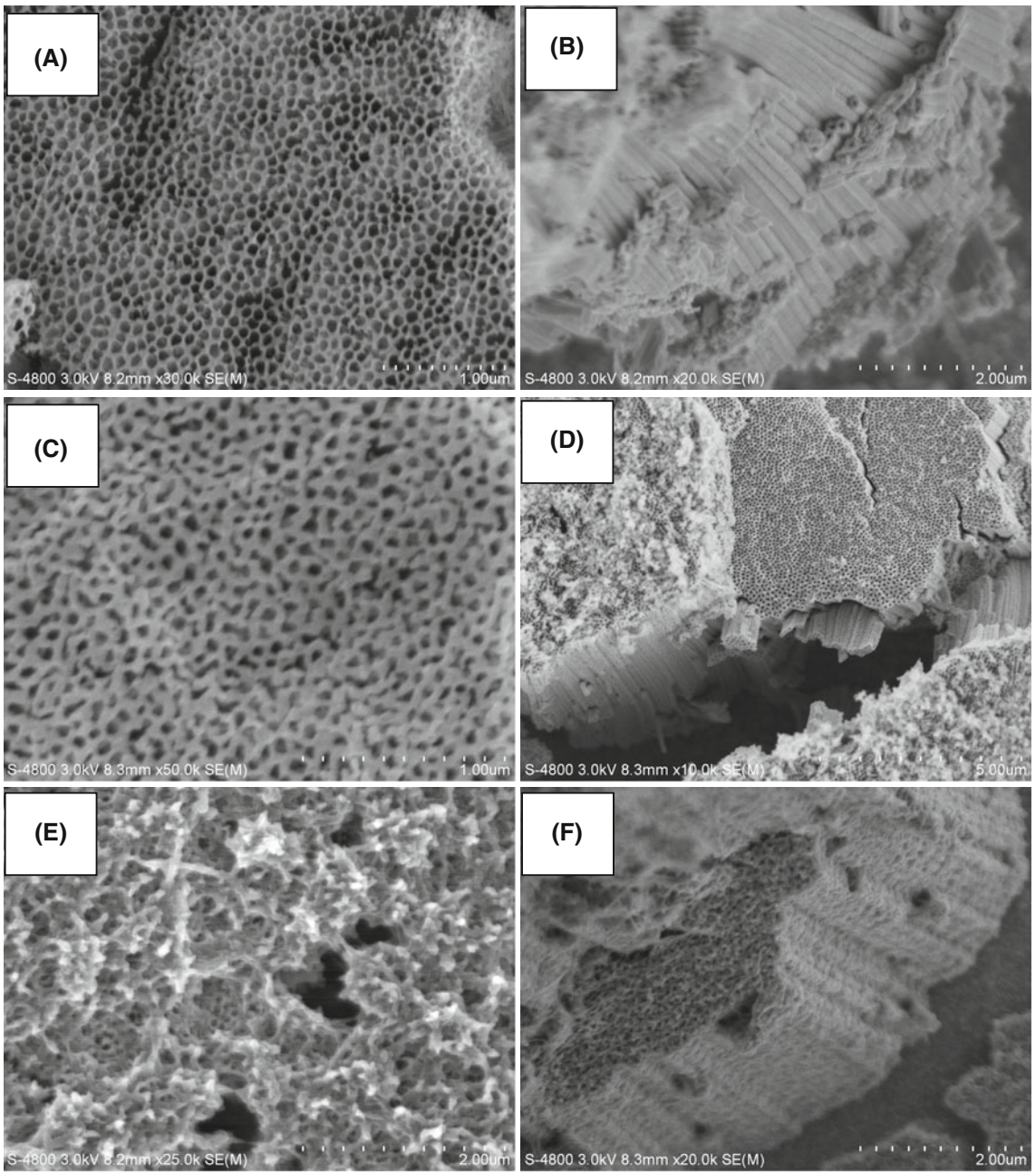

Fig. 2 *Top* view and *side* view SEM images of (**a** and **b**) TiO_2 nanotube, (**c** and **d**) TiN nanotube, and (**e** and **f**) PANI/TiN nanotube hybrid

3.2 Structure analysis

Figure 3 shows the Raman spectra of the TiO_2 nanotube, TiN nanotube, and PANI/TiN nanotube hybrid. As shown in Fig. 3b, three characteristic peaks at around 396, 516, and 696 cm^{-1} are attributed to the anatase phase of TiO_2 [10]. Raman spectra of TiN nanotube do not show characteristic peaks at this excitation wavelength (see Fig. 3a). It indicates that the anatase phase TiO_2 can be converted to cubic phase TiN after annealing in NH_3 at the temperature 800 °C [13]. The characteristic vibrations of PANI/TiN nanotube hybrid can be divided into three spectral regions, which are shown in Fig. 3c. In a high frequency region, C–C stretching vibration appears at 1,624 cm^{-1}, whereas C=C stretching vibration can be observed at 1,590 cm^{-1} [26, 27]. In the mid-frequency region, C=N stretching vibrations appear dominating at 1,506 cm^{-1} corresponding to imine sites in emeraldine form of PANI [26]. In addition, the existence of the peak at 1,344 cm^{-1} is inherently associated with the protonation process, which results from polysemiquinone radical formation. It is direct proof of PANI in its conducting state [28]. In a spectral region

below 1,210 cm^{-1}, C–H bending vibrations of aromatic rings appear at 1,169 cm^{-1}. Through these observations, it can be concluded that PANI has been fully coated onto the TiN nanotube to form a PANI/TiN nanotube hybrid.

Figure 4 shows XRD patterns of TiO_2 and TiN nanotube array. As shown in Fig. 4a, the characteristic peaks at $2\theta = 25.5°$ of *h k l* (101) and 47.5° of *h k l* (200) planes are attributed to the characteristic peaks of the anatase TiO_2 [7, 29]. As shown in Fig. 4b, the TiN nanotube array exhibits new characteristic peaks at $2\theta = 36.9°$ of *h k l* (111), 43.1° of *h k l* (200), and 62.6° of *h k l* (220) planes, which match well with the cubic TiN [12, 30]. The absence of characteristic diffraction peaks of TiO_2 in TiN indicates the full conversion of anatase TiO_2 into cubic TiN. This is consistent with the previous Raman analysis result.

3.3 Electrochemical properties

The electrochemical properties of the PANI/TiN nanotube hybrid are evaluated through cyclic voltammetry (CV) and galvanostatic charge–discharge measurement. Figure 5 shows CV curves in the applied potential range of 0-0.6 V at different scan rates. At a low scan rate from 5 to 25 mV s^{-1}, the CV curves of PANI/TiN nanotube hybrid have nearly rectangular shape. The anodic peak occurring at 0.22 V could be attributed to the transition of PANI from the semiconducting state to the conducting state [25]. Generally, the pseudo-capacitance of PANI is due to the redox reaction involving counter-ion influx and outflow from the polymer [31]. The scan rate imposes a direct impact on the diffusion of H^+ ion into the PANI. At a higher scan rate from 50 to 100 mV s^{-1}, the H^+ ion will only approach the outer surface of the electrode material. The inner pores of this electrode material will have little contribution. The pseudo-capacitance decreases and the double-layer capacitance remains accordingly.

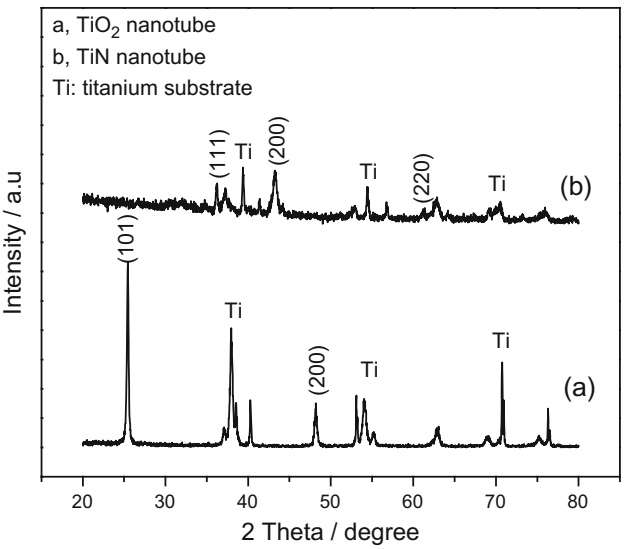

Fig. 4 XRD patterns of (**a**) TiO_2 nanotube and (**b**) TiN nanotube

Figure 6a shows the charge–discharge curves of the PANI/TiN nanotube hybrid at different current densities. The charge curves are almost linear and somewhat symmetrically mirror their discharge counterparts, indicating good electrochemical capacitance performance of the PANI/TiN nanotube hybrid. Notably, the IR drop is lower even at a high current density of 10 A g^{-1}, suggesting that the internal resistance is very low. This is due to the good electrical conductivity and ordered array construction of TiN nanotube. It is expected to facilitate a feasible electron

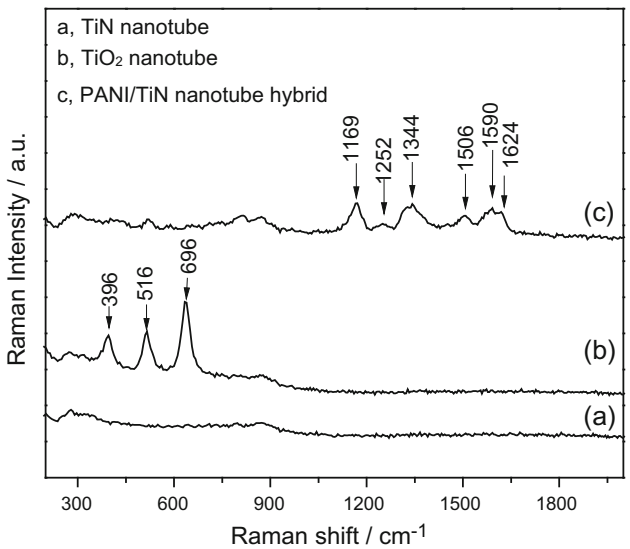

Fig. 3 Raman spectra of (**a**) TiN nanotube, (**b**) TiO_2 nanotube, and (**c**) PANI/TiN nanotube hybrid

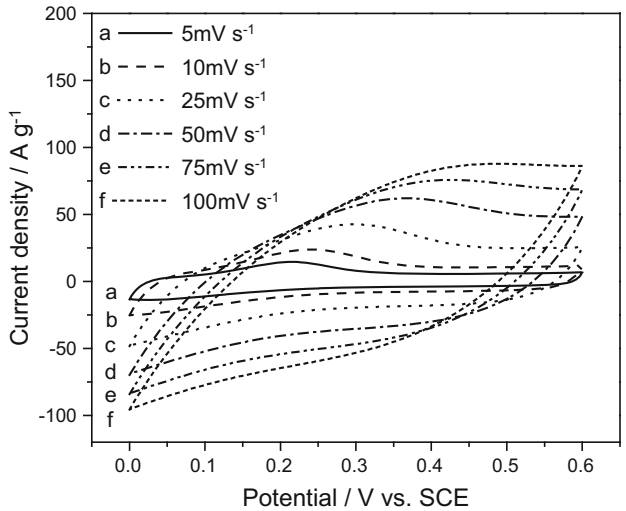

Fig. 5 Cyclic voltammetry curves of PANI/TiN nanotube hybrid at a scan rate from 5 to 100 mV s^{-1}

and ion transport. Figure 6b shows the specific capacitance as the function of the current density. The capacitance of this composite slowly decreases with the growth of current density. The specific capacitance reaches 1,066 F g^{-1} at a current density of 1 A g^{-1}. The corresponding specific capacitance still keeps at 864 F g^{-1} at a current density of 10 A g^{-1}. This capacitance is much higher than that of a previously reported PANI/TiO_2 nanotube hybrid [25]. It is believed that the PANI/TiN nanotube hybrid can become an alternative to the polyanilin/carbon nanotube array composite in supercapacitor applications [20]. The nearly ideal capacitive charge–discharge performance at a high current density of 10 A g^{-1} suggests a remarkable rate capability of this nanostructured electrode. Only 19 % capacitance loss is obtained at 10 A g^{-1} when compared with that at 1 A g^{-1}. The aligned PANI/TiN nanotube hybrid contributes a short diffusion path of reactive ions in the electrolyte solution and an effective electron transfer path along with the TiN nanotube. The fast and reversible redox reaction is achieved in a cyclic charge–discharge process. Consequently, a high electrochemical capacitance performance can be obtained for PANI/TiN nanotube hybrid when acting as supercapacitor electrode material.

The cycle stability of both TiN nanotube array and PANI/TiN nanotube hybrid was evaluated by continuous charge–discharge measurement for 200 cycles. Figure 7a and b shows that the capacitive behaviors of TiN nanotube and PANI/TiN nanotube hybrid are fully reversible. The linear symmetric charging and discharging profiles demonstrate fast charge transfer and redox kinetics. Figure 7c shows that TiN substrate keeps good stability in the 1 M H_2SO_4 aqueous solution. After 200 cycles, the specific capacitance of TiN can keeps 96 % of the initial capacity. Herein, PANI is deposited on the TiN nanotube array to achieve an integrated hybrid structure between PANI and TiN. The ordered TiN nanotube array has good electrical conductivity and high surface areas. Meanwhile, the PANI conducts a reversible redox reaction to contribute a high energy density. As shown in Fig. 7c, the specific capacitance of PANI/TiN declines from 864 to 810 F g^{-1} during the first 100 cycles, which presents 94 % retention of initial capacity. The capacitance decay during the initial charge–discharge cycles is related to the segmental detachment of the PANI layer from the top surface of the TiN nanotube. The retained specific capacitance still keeps 93 % of the initial capacity even after 200 cycles. It is noteworthy that the PANI/TiN nanotube hybrid electrode material exhibits a satisfying stability and durability in a cyclic charge–discharge process.

To further investigate the interfacial property of PANI/TiN nanotube hybrid, EIS measurements were carried out. Figure 8a shows Nyquist plots and the corresponding fitting curves of the PANI/TiN nanotube hybrid in 1 M

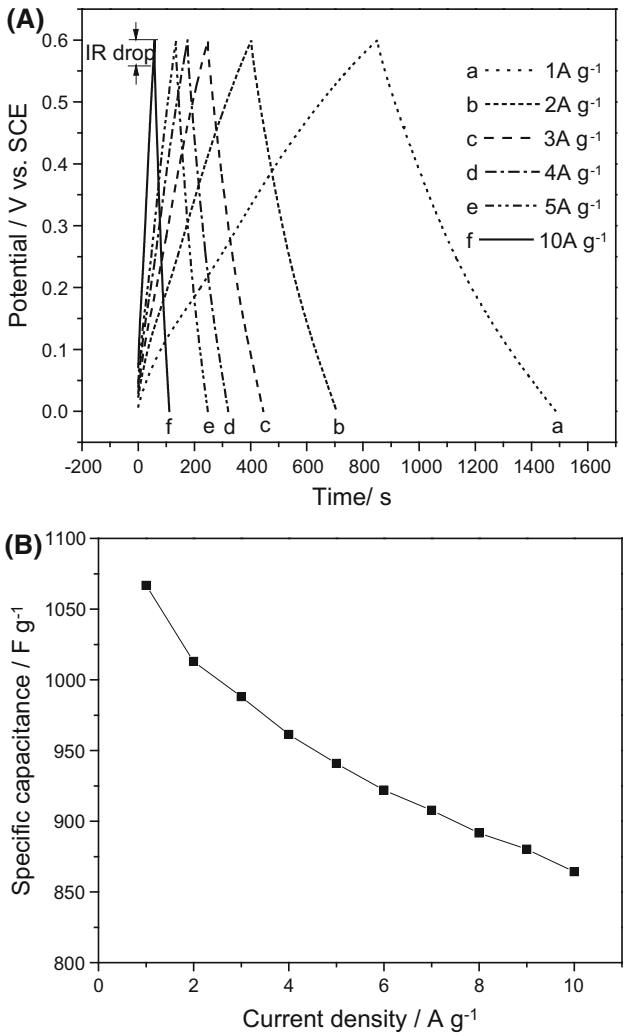

Fig. 6 **a** Galvanostatic charge–discharge curves of PANI/TiN nanotube hybrid at different current densities and **b** the specific capacitance as a function of the current density

H_2SO_4. The enlarged plot at the high frequency region is shown in the insert. The impedance plot does not exhibit a semi-circle shape, presenting the fast charge transfer of ions [31]. It benefits from the good electrical conductivity and ordered structure of TiN nanotube. To explain the inclination from the vertical line, non-homogeneity of the film and the low mobility of the proton inside the electrodes may be considered [32]. It is observed that the slope at open potential of 0 V is less than that at 0.5 V. It hints that the movement of H^+ inside the film is slower at 0 V than that at 0.5 V. It is attributed to the transition of the semiconducting state of PANI to the conducting state when the potential is transferred from 0 to 0.5 V.

The equivalent circuit for the above Nyquist diagram is presented in Fig. 8b. The equivalent circuit involves elements [31, 32] which include bulk solution resistance (R_s), a charge-transfer resistance (R_{ct}), and constant phase

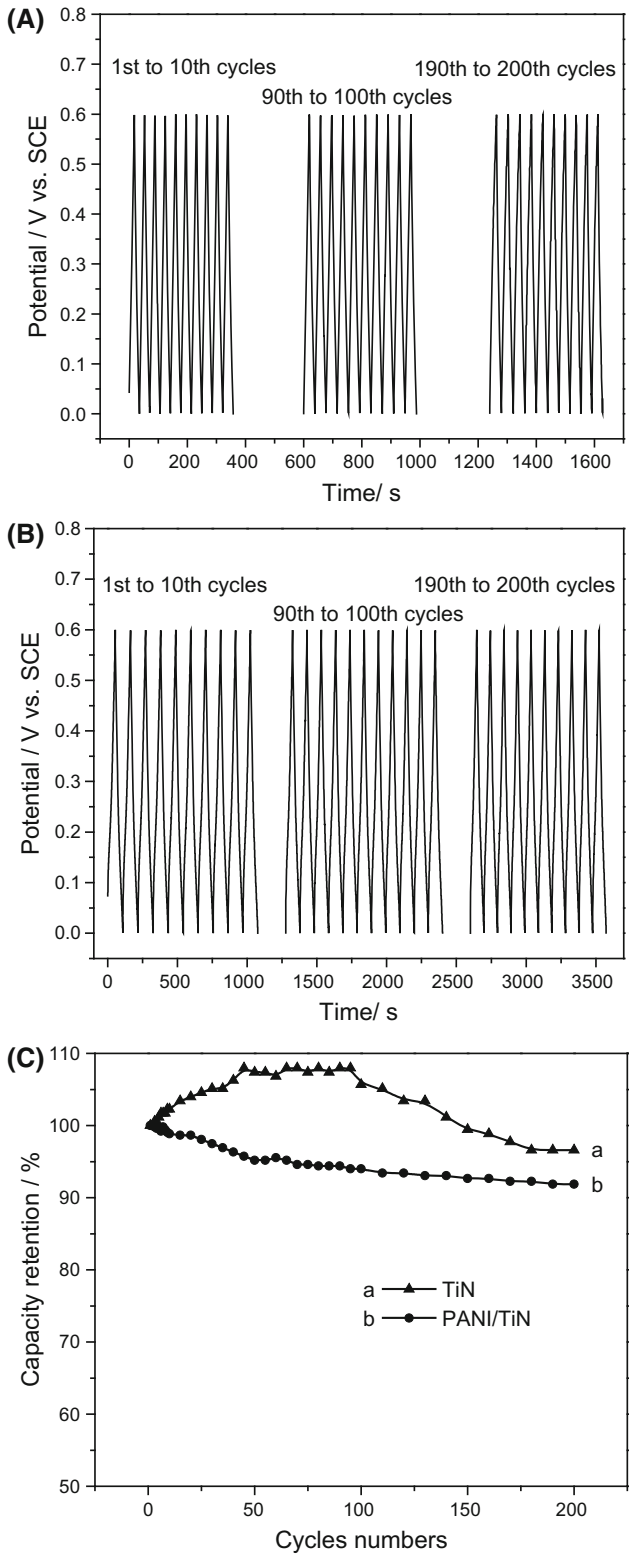

Fig. 7 Galvanostatic charge–discharge curves during 200 cycles of **a** TiN nanotube and **b** PANI/TiN nanotube hybrid; **c** the cycle stability of TiN nanotube and PANI/TiN nanotube hybrid

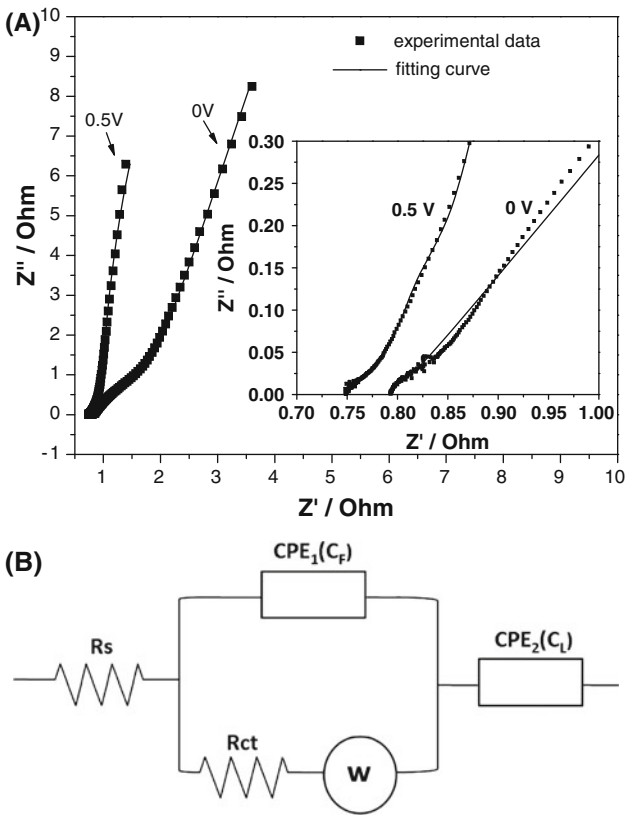

Fig. 8 **a** Nyquist plots and fitting curves of the PANI/TiN nanotube hybrid in 1 M H_2SO_4 (Enlarged plots at high frequency region as shown in the *insert*); **b** the corresponding EIS equivalent circuit

elements (CPE). CPE has been used to describe both double-layer capacitance CPF2 (C_L) and pseudo-capacitance CPE1 (C_F) in all equivalent circuit models. In addition, a Warburg diffusion element (W) is attributable to the anions' insertion in and out of the PANI polymer film in H_2SO_4 electrolyte. The fitting curves of the equivalent circuit are obtained using the Zview software. The fitting values of the equivalent circuit elements are listed in Table 1. The good fitting results imply that the equivalent circuit model reasonably reflects the electrochemical process occurring on the PANI/TiN nanotube hybrid electrode. Based on the previous literature reports, the impedance of the CPE and W can be defined by using the following equation [33–35]:

$$Z_{CPE} = \frac{1}{(CPE_T)(i\omega)^{CPE_P}} \tag{4}$$

$$Z_W = \frac{(W_R)\coth\left[(i\omega W_T)^{W_P}\right]}{(i\omega W_T)^{W_P}} \tag{5}$$

Herein, the ω is the angular frequency and i is the imaginary number. The CPE is defined by two values.

Table 1 Fitting values of the equivalent circuit elements of PANI/TiN nanotube hybrid tested at an open potential of 0 V and 0.5 V

Equivalent circuit elements	Fitting values at a different open potential (vs. SCE)	
	0 V	0.5 V
Rs (Ω)	0.78714	0.74718
CPE1-T	0.4285	1.358
CPE1-P	0.61954	0.67977
Rct (Ω)	0.02296	0.037706
CPE2-T	0.98597	2.208
CPE2-P	0.60837	0.81336
W-R	0.99814	0.06958
W-T	4.438	1.144
W-P	0.62882	0.72179

CPE-T is the capacitance when CPE-P = 1 [33, 34]. CPE-P is the constant phase element exponent, which is related to the rougher surface [34, 35]. The smaller CPE-P value is related to the rougher surface. The W is defined by three values. W-R is the diffusion resistance and the W-T is the diffusion time constant. The W-P is a fractional exponent, which has a value near 0.5 with regard to the finite length diffusion characteristic. Both the W-R and W-T decrease at a more positive open potential because of the transition of PANI from the semiconducting state to the conducting state [33, 35]. As listed in Table 1, the value of Rct is even lower than 40 mΩ. It indicates an efficient charger transfer. In addition, the small value of the Warburg impedance is indicative of a fast diffusion of doping and undoping of anions occurring inside the PANI film. Herein, the increased redox reaction rate and the fast charge transfer resulting in a uniform distribution of charge on the chains of PANI might account for the good stability of the pseudo-capacitance of the PANI/TiN nanotube hybrid electrode in the H_2SO_4 electrolyte.

In order to examine the pseudo-capacitance performance of the PANI/TiN nanotube hybrid electrode material in supercapacitor applications, an aqueous symmetric capacitor is constructed using two of the same PANI/TiN nanotube hybrid electrodes and 1 M H_2SO_4 electrolyte solution. Figure 9a shows CV curves of the symmetric supercapacitor at scan rates from 5 to 100 mV s^{-1}. The CV curve of a supercapacitor exhibits a symmetric characteristic at zero current and approaches a rectangular shape. It does not show any redox peak in the applied potential from 0 to 0.6 V vs SCE. Figure 9b shows the galvanostatic charge–discharge profiles of the symmetric supercapacitor at a current density from 1 to 5 A g^{-1}. The linear symmetric charging and discharging profiles indicate that the capacitive behavior is fully reversible. The corresponding specific capacitance and energy storage properties are

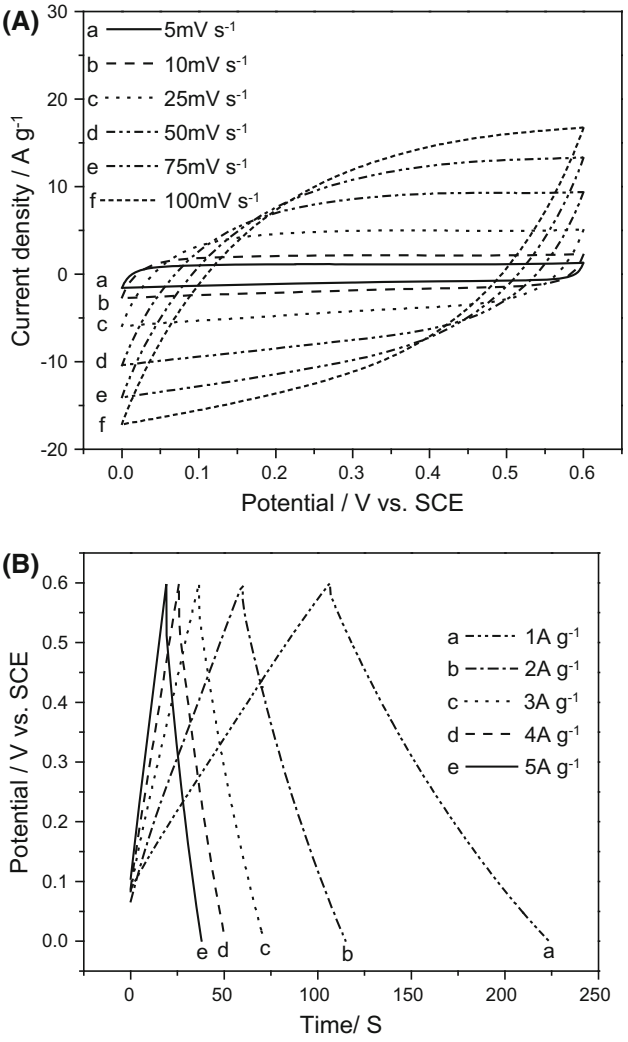

Fig. 9 **a** CV curve at different scan rates and **b** galvanostatic charge–discharge curves at different current densities of aqueous symmetric supercapacitor of PANI/TiN nanotube hybrid in 1 M H_2SO_4

Table 2 Specific capacitance, power density, and energy density of aqueous symmetric PANI/TiN supercapacitor at different current densities

Current density (A g^{-1})	Specific capacitance (F g^{-1})	Energy density (Wh kg^{-1})	Power density (kW kg^{-1})
1	194.8	9.74	0.3
2	183.3	9.165	0.6
3	173.5	8.675	0.9
4	165.3	8.265	1.2
5	156.7	7.835	1.5

listed in Table 2. The specific capacitance, specific density, and power density of the aqueous symmetric supercapacitor of PANI/TiN nanotube hybrid are 194.8 F g^{-1}, 9.74 Wh kg^{-1}, and 0.3 kW kg^{-1}, respectively, at a current

density of 1 A g^{-1} and potential window of 0.6 V. So, the PANI/TiN nanotube hybrid can act well as a supercapacitor electrode material for capacitive energy storage.

4 Conclusions

A facile method is developed to coat PANI onto a TiN nanotube array from a PANI/TiN nanotube hybrid with a coaxial nanoarray structure via a normal pulse voltammetry deposition process. The PANI/TiN nanotube hybrid has relatively high conductivity and good electroactivity. The low internal resistance promotes the efficient and fast charge-transfer framework. The ordered PANI/TiN nanotube hybrid shows a high capacitance of 1,066 F g^{-1} at a current density of 1 A g^{-1}. The capacitance retention still keeps at 93 % after 200 cycles, presenting a good cycle life. Furthermore, an aqueous symmetric supercapacitor, consisting of two of the same PANI/TiN nanotube hybrid electrodes, yields specific capacitances of 194.8 F g^{-1}, energy density of 9.74 Wh kg^{-1}, and power density of 0.3 kW kg^{-1} at a potential window of 0.6 V. These findings could open up a new approach for the PANI/TiN nanotube hybrid in supercapacitors and other electrochemical energy storage applications.

Acknowledgments The work was supported by the National Natural Science Foundation of China (No. 21373047 and 20871029), the Research Fund for the Doctoral Program of Higher Education of China (No. 200802861071), the Program for New Century Excellent Talents in University of the State Ministry of Education (No. NCET-08-0119), the Science & Technology Program of Suzhou City (No. SYG201017, ZXG2012026, SYN201208), and the Open Research Fund of State Key Laboratory of Bioelectronics, Southeast University.

References

1. Simon P, Gogotsi Y (2008) Nat Mater 7:845–854
2. Miller JR, Simon P (2008) Science 321:651–652
3. Kim JH, Zhu K, Yan Y, Perkins CL, Frank AJ (2010) Nano Lett 10:4099–4104
4. Mole F, Wang J, Clayton DA, Xu C, Pan S (2012) Langmuir 28:10610–10619
5. Lu X, Wang G, Zhai T, Yu M, Gan J, Tong Y, Li Y (2012) Nano Lett 12:1690–1696
6. Dong S, Chen X, Gu L, Zhou X, Li L, Liu Z, Han P, Xu H, Yao J, Wang H (2011) Energy Environ Sci 4:3502–3508
7. Salari M, Aboutalebi SH, Konstantinov K, Liu HK (2011) Phys Chem Chem Phys 13:5038–5041
8. Xia X, Tu J, Zhang Y, Wang X, Gu C, Zhao X, Fan HJ (2012) ACS Nano 6:5531–5538
9. Xu J, Wang K, Zu SZ, Han BH, Wei Z (2010) ACS Nano 4:5019–5026
10. Salari M, Konstantinov K, Liu HK (2011) J Mater Chem 21:5128–5133
11. Wang D, Liu Y, Wang C, Zhou F, Liu W (2009) ACS Nano 3:1249–1257
12. Qiu Y, Gao L (2005) J Phys Chem B 109:19732–19740
13. Lu X, Wang G, Zhai T, Yu MH, Xie S, Ling Y, Liang C, Tong YX, Li Y (2012) Nano Lett 12:5376–5382
14. Wang K, Zou W, Quan B, Yu A, Wu H, Jiang P, Wei Z (2011) Adv Energy Mater 1:1068–1072
15. Feng XM, Li RM, Ma YW, Chen RF, Shi NE, Fan QL, Huang W (2011) Adv Funct Mater 21:2989–2996
16. Cao Y, Mallouk TE (2008) Chem Mater 20:5260–5265
17. Nyholm L, Nyström G, Mihranyan A, Strømme M (2011) Adv Mater 23:3751–3769
18. Estaline Amitha F, Leela Mohana Reddy A, Ramaprabhu S (2009) J of Nanopart Res 11:725-729
19. Liu Q, Nayfeh MH, Yau ST (2010) J Power Sources 195:7480–7483
20. Zhang H, Cao G, Wang Z, Yang Y, Shi Z, Gu Z (2008) Electrochem Commun 10:1056–1059
21. Pushparaj VL, Shaijumon MM, Kumar A, Murugesan S, Ci L, Vajtai R, Linhardt RJ, Nalamasu O, Ajayan PM (2007) P Natl Acad Sci 104:13574–13577
22. González JR, Alcántara R, Nacimiento F, Ortiz GF, Tirado JL, Zhecheva E, Stoyanova R (2012) J Phys Chem C 116:20182–20190
23. Xie Y, Du H (2012) J Solid State Electrochem 16:2683–2689
24. Bian C, Yu A, Wu H (2009) Electrochem Commun 11:266–269
25. Mujawar SH, Ambade SB, Battumur T, Ambade RB, Lee SH (2011) Electrochim Acta 56:4462–4466
26. Patil D, Shaikh J, Dalavi D, Kalagi S, Patil P (2011) Mater Chem Phys 128:449–455
27. Liu J, Sun J, Gao L (2010) J Phys Chem C 114:19614–19620
28. Delvaux M, Duchet J, Stavaux PY, Legras R, Demoustier-Champagne S (2000) Synthetic Met 113:275–280
29. Bi Z, Paranthaman MP, Menchhofer PA, Dehoff RR, Bridges CA, Chi M, Guo B, Sun XG, Dai S (2012) J Power Sources 222:461–466
30. Han P, Yue Y, Wang X, Ma W, Dong S, Zhang K, Zhang C, Cui G (2012) J Mater Chem 22:24918–24923
31. Zou W, Wang W, He B, Sun M, Wang M, Liu L, Xu X (2010) J Electroanal Chem 641:111–118
32. Marmisollé W A, Inés Florit M, Posadas D (2012) J Electroanal Chem 673:65–71
33. Farsi H, Gobal F, Raissi H, Moghiminia S (2010) J Solid State Electrochem 14:643–650
34. Sugimoto W, Iwata H, Yokoshima K, Murakami Y, Takasu Y (2005) J Phys Chem B 109:7330–7338
35. Zhong M, Song Y, Li Y, Ma C, Zhai X, Shi J, Guo Q, Liu L (2012) J Power Sources 217:6–12